Stable Optical Trap from a Single Optical Field Utilizing Birefringence

Robinjeet Singh,[1,*] Garrett D. Cole,[2,3] Jonathan Cripe,[1] and Thomas Corbitt[1]
[1]Department of Physics & Astronomy, Louisiana State University, Baton Rouge, Louisiana, 70808
[2]Vienna Center for Quantum Science and Technology (VCQ), Faculty of Physics, University of Vienna, A-1090 Vienna, Austria
[3]Crystalline Mirror Solutions LLC and GmbH, Santa Barbara, California, 93101, USA and 1010 Vienna, Austria
(Received 10 July 2016; published 18 November 2016)

We report a stable double optical spring effect in an optical cavity pumped with a single optical field that arises as a result of birefringence. One end of the cavity is formed by a multilayer $Al_{0.92}Ga_{0.08}As/GaAs$ stack supported by a microfabricated cantilever with a natural mode frequency of 274 Hz. The optical spring shifts the resonance to 21 kHz, corresponding to a suppression of low frequency vibrations by a factor of about 5 000. The stable nature of the optical trap allows the cavity to be operated without any external feedback and with only a single optical field incident.

DOI: 10.1103/PhysRevLett.117.213604

Cavity optomechanics, the interaction of radiation pressure with movable optical elements, is an important field of study in gravitational-wave interferometers [1–3] and in probing quantum mechanics with macroscopic systems [4–10]. It is well established that in an optomechanical cavity, the radiation pressure due to the circulating field can act as a (anti-)restoring and (anti-)damping force, depending on whether the cavity is red or blue detuned [1,11–13]. The (anti-)restoring force is generated by the position-dependent intracavity power and radiation pressure, while the (anti-)damping force is due to the finite response time of the cavity to changes of the mirror position.

If the cavity length is adjusted so that its resonant frequency is less than the laser frequency (blue detuned), the radiation pressure gives rise to a positive restoring force and an antidamping force. Likewise, when red detuned, antirestoring and positive damping forces are generated. For systems in which the optical forces dominate their mechanical counterparts, this leads to instability from either an antirestoring or antidamping force. The relative signs of the restoring and damping may be modified when operated in the resolved-sideband regime [9], but here we focus on the regime in which the optical spring is much stronger than the mechanical stiffness, and the resulting optical spring resonance is at a lower frequency than the cavity linewidth. The optical spring formed by a restoring force has a profound effect in systems with soft mechanical suspensions and can be used to enhance the sensitivity of detection by amplifying the mirror's motion. The strong antidamping force can dominate the mechanical damping in this scenario giving rise to dynamic instabilities [2,14,15] and is usually stabilized by actively controlling the optical response of the cavity through feedback loops [2,14].

In 2007, Corbitt *et al.* [16] introduced a dual carrier stable optical trap in which a damping force due to a red detuned subcarrier field cancels out the antidamping force due to the blue detuned carrier field [16]. That approach eliminated the need for electronic feedback but required using two distinct optical fields incident on the cavity. Recently, a new approach that exploits the bolometric backaction due to the photothermal effect was proposed by Kelley *et al.* [17]. This approach produces a damping force by exploiting the thermal expansion of the mirrors from absorption of the intracavity optical field. Though stable, such optical absorption introduces excess vacuum fluctuations and deteriorates the sensitivity of the device.

In this Letter, we introduce a new scheme to achieve a stable optical trap by exploiting the birefringence inherent to the mirrors, without relying on absorption or multiple carrier fields. We inject a single field with linear polarization into the cavity. The cavity consists of a 0.5-in. input mirror and a microfabricated mirror supported on a cantilever as the end mirror. The microresonator is fabricated from a stack of crystalline $Al_{0.92}Ga_{0.08}As/GaAs$ layers and is inherently birefringent, resulting in differing resonance conditions for the orthogonal polarizations. The observed birefringence is in part a consequence of the finite lattice mismatch in the high and low index layers of the epitaxially grown distributed Bragg reflector structure of the microresonator [18,19]. The fabrication of the microresonator is described in the Supplemental Material [20].

The two polarization components of the input field undergo a relative phase shift as a function of the birefringence. This phase shift allows the two polarization components to operate at different cavity detunings, which gives rise to the stable double optical spring. We note that the phase shifted polarizations behave as if there were two input fields. We will refer to these orthogonal polarization components as the carrier (C) and the subcarrier (SC) polarizations, for convenience.

The schematic shown in Fig. 1 describes the experiment performed to demonstrate our scheme. Initially, the intensity

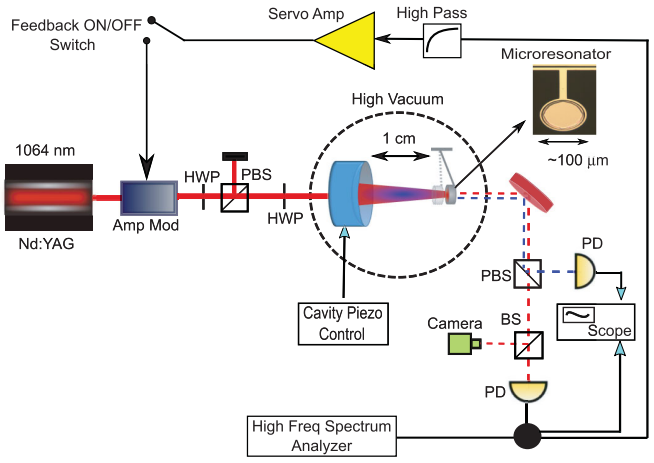

FIG. 1. Experimental setup: A 1064-nm Nd:YAG laser outputs 500 mW of near infrared light. The intensity of the input laser field is controlled by the amplitude modulator through a high pass feedback control loop. The first half wave plate (HWP) and a polarization beam splitter (PBS) set the total coupled power of the input laser field to about 42 mW, and the second HWP controls the power ratio between the carrier (C) and subcarrier (SC) polarization components of the input field to about 22:1. The cavity is located inside a vacuum tank and consists of a 0.5-in.-diameter input mirror and the 100-μm-diameter microresonator (inset). The transmitted signals from the carrier (red) and the subcarrier (blue) components are separated by a PBS. A 90:10 beam splitter (BS) splits the carrier transmission for signal detection by a photodetector and for qualitative detection by a camera. The carrier photodetector signal is used for signal analysis and as an error signal for the feedback control.

of the laser field from the Nd:YAG laser is modulated by an amplitude modulator through a servocontrolled feedback signal from the transmitted cavity output field. The feedback provides a damping force to stabilize the optical spring while it is in the unstable region, and it only acts in a narrow frequency band around the optical spring resonance. The optical spring suppresses the cavity fluctuations below the optical spring resonance, up to a maximum factor of about 5 000 at low frequencies, as determined by the ratio of the optical spring constant to the mechanical spring constant. That reduction stabilizes the cavity and allows for long-term operation without feedback at low frequencies. The polarization angle of the input field is set using a combination of two half wave plates and a polarizing beam splitter, such that the power in the C polarization is about 22 times the power in the SC polarization. The input power coupled to the cavity in C and SC polarizations is about 40.1 and 1.9 mW, respectively.

The in-vacuum cavity is 1 cm long and consists of an input mirror that has a radius of curvature of 1 cm. The input mirror is mounted on a piezoelectric device to allow for fine-tuning of the cavity length. The optical field is focused on a microresonator that is about 100 μm in diameter and about 400 ng in mass. The microresonator has a natural mechanical frequency of $\Omega_m = 2\pi \times 274$ Hz with a mechanical quality factor $Q_m \approx 2 \times 10^4$. The birefringence-induced frequency shift of the resonance condition between the two polarizations in our experiment is measured to be about 7.4 times the cavity linewidth (HWHM) of $\gamma \approx 2\pi \times 254$ kHz.

The transmitted field from the end mirror is used to qualitatively analyze the cavity modes, determine the cavity noise spectrum, and to generate a feedback error signal for the initial control of the cavity. The C and the SC components of the transmitted fields are separated using a polarizing beam splitter, and the amplitude of the SC transmission is measured by a photodetector. The transmitted C polarization is further split by a 90:10 beam splitter for which 10% of the signal is detected by a CCD camera in order to realize a qualitative analysis of the cavity modes. The rest of the C transmission is detected by a photodetector and is used both for the initial feedback control and the signal analysis of the cavity features. The electronic feedback control of the intensity of the input field is turned off once the self-stable regime is reached.

The power inside the cavity and the resulting radiation pressure on the microresonator test mass depend on the resonance condition of the cavity. For a large cavity linewidth, we take the frequency of motion $\Omega \ll \gamma$, such that the associated oscillatory spring constant is given by [17]

$$K_{\mathrm{os}} = \frac{16\pi P_{\mathrm{in}} T_1 \sqrt{R_1 R_2^3}}{c\lambda_0 (1-\sqrt{R_1 R_2})^3} \frac{\delta_\gamma}{(1+\delta_\gamma^2)^2}, \tag{1}$$

where P_{in} is the input power of the laser field. T_i and R_i are the transmittance and the reflectance of the input mirror ($i = 1$) and the end test mass ($i = 2$), $\delta_\gamma = \delta/\gamma$ is the field detuning in terms of the cavity linewidth, λ_0 is the center wavelength of the input laser field, and c is the velocity of light.

In addition, the detuned cavity has a finite response time on the scale of γ^{-1}, and, hence, the response of the intracavity power lags the mirror motion. This lag, in effect, leads to a viscous damping force with a damping coefficient given by Refs. [11,14], again under the assumption that $\Omega \ll \gamma$,

$$\Gamma = \frac{-2K_{\mathrm{os}}}{M\gamma[1+\delta_\gamma^2]}, \tag{2}$$

where M is the reduced mass of the two cavity mirrors. Compared with the fixed mirror, the microresonator has a negligible mass, and, hence, the reduced mass is simply equal to the mass of the cantilever.

For the optomechanical dynamics to be stable, a positive spring constant ($K > 0$) and a positive damping coefficient ($\Gamma > 0$) are required. But as is evident from the dependence of K and Γ on the sign of δ [Eqs. (1) and (2)], a positive (restoring) spring constant implies instabilities due to negative damping force under the assumption that $\Omega \ll \gamma$.

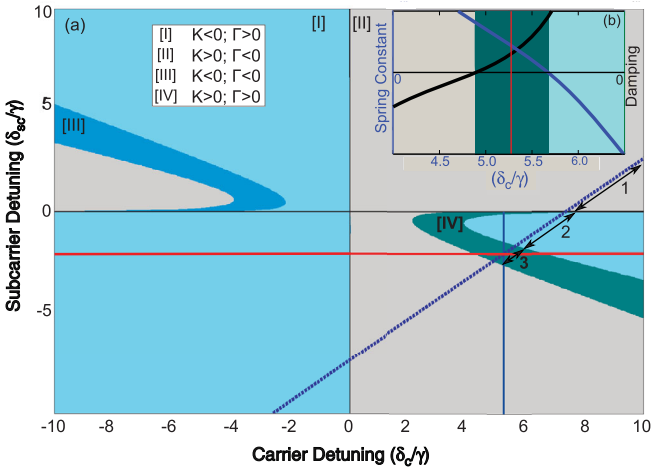

FIG. 2. Graphical representation for the total optical rigidity as a function of detunings of the carrier C and subcarrier SC at a fixed input power ratio of 22:1, respectively. The shaded regions [I], [II], [III], and [IV], respectively, correspond to a statically unstable region with $K < 0$ and $\Gamma > 0$, dynamically unstable region with $K > 0$ and $\Gamma < 0$, antistable region with $K < 0$ and $\Gamma < 0$, and stable region with $K > 0$ and $\Gamma > 0$. The dotted blue line represents the trajectory of the C over the cavity resonance and agrees with both the calculated and the experimentally measured data. Regions 1, 2, and 3 on the trajectory of C are in direct correspondence with the real time sweep data as shown in Fig. 3. A stable optical trap is achieved at $\delta_C/\gamma \sim 5.3$ and $\delta_{SC}/\gamma \sim -2.1$. The inset (b) shows the spring constant and damping as a function of δ_C/γ, K, and Γ where the vertical red line represents the stable optical trap from the experimental data.

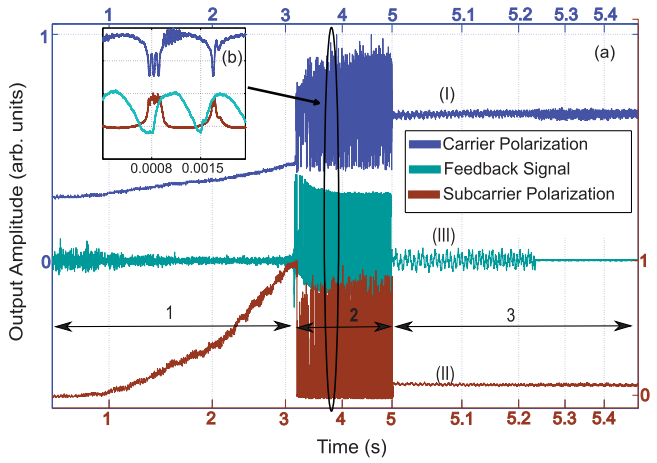

FIG. 3. The real time sweep data showing the output signal for the C polarization (I), the SC polarization (II), and the feedback to the amplitude modulator (III). Region 1 of the plot shows the rise in the amplitude for the C and the SC polarizations, as they scan up the resonant cavity. The oscillations as a result of static instabilities are shown in region 2 of the plot and are magnified in the inset plot (b). Region 3 of the plot shows the system being stable and independent of the feedback control, as shown in region of the plot where the feedback is turned off.

This instability due to negative damping usually requires feedback control.

In our experiment, the system is stabilized by adjusting the detuning of the C and SC components of the intracavity field such that the blue detuned C polarization component creates a large restoring force and only small antidamping force, while the red detuned SC polarization creates a small antirestoring force and a large damping force. The reflectivities of the mirrors are the same for both polarizations in this system, as determined by optical ringdown measurements. At detunings of $\delta_C \approx 5.3\gamma$ and $\delta_{SC} \approx -2.1\gamma$, the intracavity carrier and subcarrier polarization component fields interact with the mechanical system resulting in $K_{tot} \Rightarrow K_{os}^{C} + K_{os}^{SC} > 0$ and $\Gamma_{tot} \Rightarrow \Gamma_C + \Gamma_{SC} > 0$.

Figure 2 depicts the numerical model for the operating regimes of our system at a fixed input coupled power of 42 mW. The total optical rigidity due to the two polarization field components is plotted as a function of carrier and the subcarrier detunings. The numerical model is in agreement with our experimentally observed stable optical trap, as can be seen from the locking acquisition of our optomechanical system (Fig. 3). The blue dotted line in Fig. 2 corresponds to the locking acquisition in Fig. 3 where the amplitudes for the transmission of the carrier (I), subcarrier (II), and the feedback control signal are shown. The feedback control signal is designed to provide a damping force and is capable of counteracting the optical antidamping that is dominant during initial locking, which is shown as region 1 in Figs. 2 and 3. When the system enters region 2, the SC crosses onto the other side of the resonance and exerts a strong antirestoring force. The feedback is unable to counteract an antirestoring force, and the system oscillates. As the SC detuning increases and the system moves into region 3, the optomechanical dynamics stabilizes as the restoring force from the C exceeds the antirestoring force of the SC. At this point, the feedback loop is turned off, and the system remains locked and stable. This does result in slightly higher vibration levels in the absence of the damping feedback loop.

Figure 2(b) depicts the sign of the total spring constant and the damping coefficient due to the two polarization components as a function of carrier detuning around the stable optical trap region. The results further correspond to the experimental measurement for the optical spring response at a polarization-dependent stable optical trap discussed above.

As shown in Fig. 4, the mechanical resonance of the microresonator is shifted from 274 Hz to about 21 kHz. The optical trap is stable, as can be seen from the decrease in the phase, allowing the system to be operated without any feedback control. The fluctuations of the optically trapped mirror are relatively large in the performed measurement regime, and there are some nonlinearities that are contributing to the noise in this measurement. Figure 4 shows the

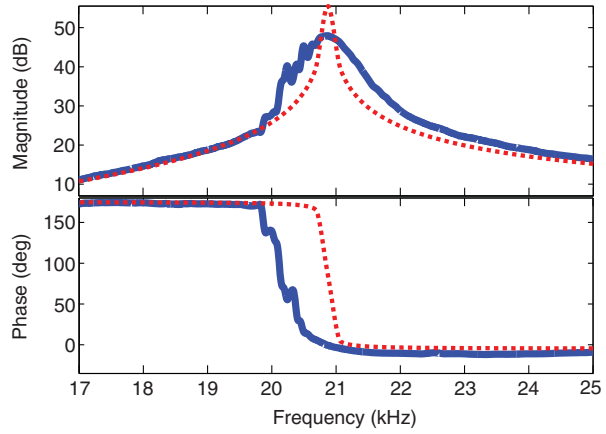

FIG. 4. The measured transfer function of a signal sent to the amplitude modulator to the transmission photodetector of the carrier is shown (blue), along with the calculated optical response (dotted red). We note that this measurement is performed open loop, where the feedback signal to the amplitude modulator is turned off here and the cavity is self-stabilized as a result of an optical trap. The disagreement between the measured and calculated Q is attributed to the fact that the resulting vibrations in the system are sufficient to jitter the intracavity power and modulate the optical spring frequency in the time that it takes to perform this measurement.

effects of such fluctuations on the measured transfer function of the oscillator as compared to the calculated transfer function. We have verified that this stabilization is due to polarization and not other effects, such as photothermal effects, by confirming the polarization dependence on the observed stability. We note that by varying the input polarization angle and, hence, the power in the C and the SC, the observed stability region shifts in agreement with the expected shifts in the detunings of the C and the SC polarizations and lies in the stable region IV of Fig. 2.

In conclusion, we have demonstrated a polarization-dependent stable optical trap for a microresonator-based optomechanical system, as the outcome of a strong optical spring and optical damping. The dynamics of the system are controlled by radiation pressure and depend on the detunings of the polarization components of the input field. We have experimentally demonstrated the stability of the system and confirmed that the deactivation of the feedback control does not render the system unstable. We believe our scheme to be a useful technique for manipulating and stabilizing the dynamics of the vast variety of optomechanical systems.

Because of the simplicity of the technique, the polarization-based optical trapping technique has many potential applications in high sensitivity optomechanical systems. Since our technique does not depend on absorption, the application can be used without degrading the quantum-limited sensitivity of the experiment.

In the present measurement, the large separation of the two polarizations leads to a smaller than desired optical spring. Thus, we note that it would be beneficial to have control over the birefringence effect, so that the difference in the detunings of the carrier and subcarrier $\delta_C - \delta_{SC}$ could be adjusted ideally to lie in the range of about 3γ. This could be accomplished if both cavity mirrors were made to be birefringent. In that case, one of the mirrors could be rotated with respect to the other, effectively tuning the splitting frequency between the neighboring polarization eigenmodes.

This work was supported by the National Science Foundation Grant No. PHY-1150531. This document has been assigned the LIGO Document No. LIGO-P1600135. The authors acknowledge D. McClelland of the ANU College of Physics and Mathematical Sciences for useful discussions and confirmation of similar effects observed in gram-scale metal flexures.

*roubein@gmail.com

[1] A. Buonanno and Y. Chen, Signal recycled laser-interferometer gravitational-wave detectors as optical springs, Phys. Rev. D **65**, 042001 (2002).

[2] O. Miyakawa *et al.*, Measurement of optical response of a detuned resonant sideband extraction gravitational wave detector, Phys. Rev. D **74**, 022001 (2006).

[3] T. Corbitt, Y. Chen, F. Khalili, D. Ottaway, S. Vyatchanin, S. Whitcomb, and N. Mavalvala, Squeezed-state source using radiation-pressure-induced rigidity, Phys. Rev. A **73**, 023801 (2006).

[4] C. H. Metzger and K. Karrai, Cavity cooling of a microlever, Nature (London) **432**, 1002 (2004).

[5] A. Naik, O. Buu, M. D. LaHaye, A. D. Armour, A. A. Clerk, M. P. Blencowe, and K. C. Schwab, Cooling a nanomechanical resonator with quantum back-action, Nature (London) **443**, 193 (2006).

[6] S. Gigan, H. R. Bohm, M. Paternostro, F. Blaser, G. Langer, J. B. Hertzberg, K. C. Schwab, D. Bauerle, M. Aspelmeyer, and A. Zeilinger, Self-cooling of a micromirror by radiation pressure, Nature (London) **444**, 67 (2006).

[7] D. Kleckner and D. Bouwmeester, Sub-kelvin optical cooling of a micromechanical resonator, Nature (London) **444**, 75 (2006).

[8] O. Arcizet, P.-F. Cohadon, T. Briant, M. Pinard, and A. Heidmann, Radiation-pressure cooling and optomechanical instability of a micromirror, Nature (London) **444**, 71 (2006).

[9] A. Schliesser, P. Del'Haye, N. Nooshi, K. J. Vahala, and T. J. Kippenberg, Radiation Pressure Cooling of a Micromechanical Oscillator Using Dynamical Backaction, Phys. Rev. Lett. **97**, 243905 (2006).

[10] I. Mahboob, H. Okamoto, K. Onomitsu, and H. Yamaguchi, Two-Mode Thermal-Noise Squeezing in an Electromechanical Resonator, Phys. Rev. Lett. **113**, 167203 (2014).

[11] V. Braginsky and S. Vyatchanin, Low quantum noise tranquilizer for Fabry-Perot interferometer, Phys. Lett. A **293**, 228 (2002).

[12] B. S. Sheard, M. B. Gray, C. M. Mow-Lowry, D. E. McClelland, and S. E. Whitcomb, Observation and

characterization of an optical spring, Phys. Rev. A **69**, 051801 (2004).
[13] S. Mancini, D. Vitali, and P. Tombesi, Optomechanical cooling of a macroscopic oscillator by homodyne feedback, Phys. Rev. Lett. **80**, 688 (1998).
[14] T. Corbitt, D. Ottaway, E. Innerhofer, J. Pelc, and N. Mavalvala, Measurement of radiation-pressure-induced optomechanical dynamics in a suspended Fabry-Perot cavity, Phys. Rev. A **74**, 021802 (2006).
[15] T. J. Kippenberg, H. Rokhsari, T. Carmon, A. Scherer, and K. J. Vahala, Analysis of Radiation-Pressure Induced Mechanical Oscillation of an Optical Microcavity, Phys. Rev. Lett. **95**, 033901 (2005).
[16] T. Corbitt, Y. Chen, E. Innerhofer, H. Müller-Ebhardt, D. Ottaway, H. Rehbein, D. Sigg, S. Whitcomb, C. Wipf, and N. Mavalvala, An All-Optical Trap for a Gram-Scale Mirror, Phys. Rev. Lett. **98**, 150802 (2007).
[17] D. Kelley, J. Lough, F. Mangaña-Sandoval, A. Perreca, and S. W. Ballmer, Observation of photothermal feedback in a stable dual-carrier optical spring, Phys. Rev. D **92**, 062003 (2015).
[18] G. D. Cole, W. Zhang, M. J. Martin, J. Ye, and M. Aspelmeyer, Tenfold reduction of Brownian noise in high-reflectivity optical coatings, Nat. Photonics **7**, 644 (2013).
[19] G. D. Cole *et al.*, High-performance near- and mid-infrared crystalline coatings, Optica **3**, 647 (2016).
[20] See the Supplemental Material at http://link.aps.org/supplemental/10.1103/PhysRevLett.117.213604, which includes Refs. [22–28], for a detailed description of the microresonator material structure and fabrication procedure.
[21] G. D. Cole, S. Gröblacher, K. Gugler, S. Gigan, and M. Aspelmeyer, Monocrystalline $Al_xGa_{1-x}As$ heterostructures for high-reflectivity high-Q micromechanical resonators in the megahertz regime, Appl. Phys. Lett. **92**, 261108 (2008).
[22] G. D. Cole, in *Cavity optomechanics with low-noise crystalline mirrors*, SPIE Proceedings 8458, edited by K. Dholakia, and G. C. Spalding (SPIE-International Society for Optical Engineering, Bellingham, 2012).
[23] F. Sugihwo, M. C. Larson, and J. S. Harris, Simultaneous optimization of membrane reflectance and tuning voltage for tunable vertical cavity lasers, Appl. Phys. Lett. **72**, 10 (1998).
[24] G. D. Cole, E. S. Bjorlin, Q. Chen, C.-Y. Chan, S. Wu, C. S. Wang, N. C. MacDonald, and J. E. Bowers, MEMS-tunable vertical-cavity SOAs, IEEE J. Quantum Electron. **41**, 390 (2005).
[25] G. D. Cole, E. Behymer, T. C. Bond, and L. L. Goddard, Short-wavelength MEMS-tunable VCSELs, Opt. Express **16**, 16093 (2008).
[26] S. Groblacher, J. B. Hertzberg, M. R. Vanner, G. D. Cole, S. Gigan, K. C. Schwab, and M. Aspelmeyer, Demonstration of an ultracold micro-optomechanical oscillator in a cryogenic cavity, Nat. Phys. **5**, 485 (2009).
[27] G. D. Cole *et al.*, Tensile-strained $In_xGa_{1-x}P$ membranes for cavity optomechanics, Appl. Phys. Lett. **104**, 201908 (2014).